Computational Materials Science 98 (2015) 417–423

Contents lists available at ScienceDirect

Computational Materials Science

journal homepage: www.elsevier.com/locate/commatsci

Lattice inversion modified embedded atom method for bcc transition metals

Xianbao Duan [a], Bing Zhou [b], Yanwei Wen [a], Rong Chen [b], Huamin Zhou [a], Bin Shan [a,c,*]

[a] State Key Laboratory of Material Processing and Die and Mould Technology and School of Materials Science and Engineering, Huazhong University of Science and Technology, Wuhan 430074, Hubei, People's Republic of China
[b] State Key Laboratory of Digital Manufacturing Equipment and Technology and School of Mechanical Science and Engineering, Huazhong University of Science and Technology, Wuhan 430074, Hubei, People's Republic of China
[c] Department of Materials Science and Engineering, The University of Texas at Dallas, Richardson, TX 75080, USA

ARTICLE INFO

Article history:
Received 7 October 2014
Received in revised form 17 November 2014
Accepted 21 November 2014

Keywords:
Lattice inversion
MEAM
Interatomic potential
Bcc transition metals

ABSTRACT

Lattice inversion modified embedded atom method (LI-MEAM), proposed as an alternative implementation of MEAM models by removing the many-body screening function and including the interactions from more nearest neighbors, was applied to the bcc transition metals, Fe, Cr, Mo, W, V, Nb, and Ta in the present work. The interatomic potential was parameterized by fitting to individual elastic constants, structural energy differences, vacancy formation energy, and surface energy using particle swarm optimization method. Various physical properties of individual elements, including structural properties, vacancy defect properties, surface properties, and thermal properties were presented along with experimental data and those calculated using the second nearest neighbor MEAM (2NN MEAM) in this article so as to evaluate the optimized parameters and verify the LI-MEAM model. It is shown that LI-MEAM potential could reasonably reproduce both the fitted and the predicted properties for all bcc transition metals.

1. Introduction

Atomistic simulations, including molecular dynamics and Monte Carlo simulations, are among the most commonly used techniques to explore the relationships between structures and the physical properties for specific materials. Compared with *ab initio* calculations, atomistic simulations are capable to investigate extremely large systems, say, more than one hundred million atoms [1,2]. By choosing appropriate interatomic potentials, it is possible to achieve relatively high accuracy of the calculated results. From this perspective, interatomic potential models play a crucial role in guaranteeing the reliability of the obtained results. Hence, it is of great importance on proposing new interatomic potential models with higher accuracy and efficiency.

In the past decades, many classical models were presented to describe the interactions among atoms or molecules [3–12]. Among the various models, the modified embedded atom method (MEAM, also for 1NN MEAM) proposed by Baskes et al. [9,10,12] stood out for its universality and accuracy, and the capability of predicting the properties of a variety of metals and alloys accurately. However, it failed to predict the ordering of low-index surface energies and also exhibited structural instabilities when being applied to some bcc transition metals [13]. Lee attributed it to the neglect of the interactions from the second nearest neighbors since the second nearest neighbors in bcc metals were relatively close to the first neighbors [13]. He thus proposed the second nearest neighbor MEAM (2NN MEAM) by additionally considering the interactions from the second nearest neighbors [13–15]. Despite the fact that the same number of parameters are used for 1NN and 2NN MEAM, 2NN MEAM does a much better job in handling a wider range of physical properties. However, either in 1NN or 2NN MEAM formalism, an additional environmental dependent many-body screening function must be used to describe the screening effects on the atoms beyond first or second nearest neighbors, which increases the complexity of the models. Besides, the screening function increases the number of parameters, especially for alloys. Along the same logic for improving the MEAM formalism from 1NN to 2NN, if the interactions from more nearest neighbors are considered, it is possible that the MEAM model could be further improved or simplified.

* Corresponding author at: State Key Laboratory of Material Processing and Die and Mould Technology and School of Materials Science and Engineering, Huazhong University of Science and Technology, Wuhan 430074, Hubei, People's Republic of China.
E-mail address: bshan@mail.hust.edu.cn (B. Shan).

http://dx.doi.org/10.1016/j.commatsci.2014.11.048
0927-0256/

As a result, we proposed an alternative MEAM formalism by removing the many-body screening function and extending further nearest neighbors with Chen–Möbius lattice inversion method, named the lattice inversion MEAM (LI-MEAM). This makes our treatment of the many-body screening essentially same as EAM and greatly simplified the physical picture. Moreover, we parameterized the potential parameters of a series of bcc metals (Cr, Mo, W, V, Nb, Ta) by particle swarm optimization method and calculated various physical properties of bulk materials to validate the developed LI-MEAM potential. The results show a good agreement with available experimental data and comparable with those of 2NN MEAM method. The outline of present work can be described as the following. Section 2 reviews the formalism of LI-MEAM potential briefly. Section 3 mainly shows the optimized potential parameters and the predicted physical properties. Section 4 is a short summary.

2. Methodology

In LI-MEAM, the total energy per atom for an arbitrary system is composed of two parts, the embedding energy and the pair energy, as:

$$E = F(\bar{\rho}_i) + \frac{1}{2}\sum_{i\neq j}\Phi(r_{ij}), \tag{1}$$

where F is the embedding function, $\bar{\rho}_i$ is the background electron density at site i, $\Phi(r_{ij})$ is the pair potential between atoms i and j at a distance r_{ij}. The embedding function, F, is given by:

$$F(\bar{\rho}) = AE_c(\bar{\rho}/\bar{\rho}^0)\ln(\bar{\rho}/\bar{\rho}^0), \tag{2}$$

where A is the scaling factor, E_c is the sublimation energy, $\bar{\rho}^0$ is the background electron density for the reference structure. Usually, for a specified element, the equilibrium structure is taken as the reference structure. For all the concerned elements in present work, bcc was chosen as the reference structure. The background electron density $\bar{\rho}_i$ in Eq. (1) is given by:

$$\bar{\rho}_i = \bar{\rho}_i^{(0)}G(\Gamma), \tag{3}$$

where

$$G(\Gamma) = 2/(1+e^{-\Gamma}), \tag{4}$$

and

$$\Gamma = \sum_{k=1}^{3} t_i^{(k)}\left(\frac{\bar{\rho}_i^{(k)}}{\bar{\rho}_i^{(0)}}\right)^2. \tag{5}$$

In the equations, $\bar{\rho}_i^{(k)}$ represent the spherical ($k=0$) and angular ($k=1, 2, 3$) electron densities. $t_i^{(k)}$ ($k=1, 2, 3$) are the corresponding weighting factors for the three angular electron densities. $\bar{\rho}_i^{(k)}$ are given by:

$$(\bar{\rho}_i^{(0)})^2 = \left[\sum_{j\neq i}\rho_j^{a(0)}\right]^2, \tag{6a}$$

$$(\bar{\rho}_i^{(1)})^2 = \sum_{\alpha}\left[\sum_{j\neq i}\frac{r_{ij}^{\alpha}}{r_{ij}}\rho_j^{a(1)}\right]^2, \tag{6b}$$

$$(\bar{\rho}_i^{(2)})^2 = \sum_{\alpha,\beta}\left[\sum_{j\neq i}\frac{r_{ij}^{\alpha}r_{ij}^{\beta}}{r_{ij}^2}\rho_j^{a(2)}\right]^2 - \frac{1}{3}\left[\sum_{j\neq i}\rho_j^{a(2)}\right]^2, \tag{6c}$$

$$(\bar{\rho}_i^{(3)})^2 = \sum_{\alpha,\beta,\gamma}\left[\sum_{j\neq i}\frac{r_{ij}^{\alpha}r_{ij}^{\beta}r_{ij}^{\gamma}}{r_{ij}^3}\rho_j^{a(3)}\right]^2 - \frac{3}{5}\sum_{\alpha}\left[\sum_{j\neq i}\frac{r_{ij}^{\alpha}}{r_{ij}}\rho_j^{a(3)}\right]^2. \tag{6d}$$

Here, $\rho_j^{a(k)}$ ($k=0, 1, 2, 3$) are the atomic electron densities of atom j for different directions. r_{ij}^{α}, r_{ij}^{β}, r_{ij}^{γ} are the α, β, γ components of r_{ij}, respectively. $\rho_i^{a(k)}$ in Eq. (6) have the following form:

$$\rho_i^{a(k)}(r_{ij}) = e^{-\beta_i^{(k)}(r_{ij}/r_e-1)}, \tag{7}$$

where $\beta_i^{(k)}$ ($k=0, 1, 2, 3$) are decay factors for corresponding atomic electron densities, r_e is the nearest neighbor distance in the equilibrium reference structure.

To obtain the form of pair potential in Eq. (1) so that the total energy for an arbitrary system can be calculated, a reference structure with known total energy per atom (or called cohesive energy) should be selected. Normally, the cohesive energy could be determined according to experimental data or *ab initio* calculations directly. Herein, the universal equation of state proposed by Rose et al. [16] is used to express the total cohesive energy per atom for the reference structure, E^u, as a function of the nearest-neighbor distance r:

$$E^u(r) = -E_c(1+a^*)e^{-a^*}, \tag{8}$$

where

$$a^* = \alpha(r/r_e - 1), \tag{9}$$

and

$$\alpha = \sqrt{9B\Omega/E_c}. \tag{10}$$

Here, B is bulk modulus. Ω is equilibrium atomic volume, which is dependent on the equilibrium nearest-neighbor distance r_e.

With the cohesive energy known, the pair energy per atom could thus be calculated by subtracting the calculated embedding energy of the same reference structure. From another point of view, the pair energy per atom can be expressed as the accumulation of the pair potentials between the surrounding neighbors and the reference atom. In practice, 1NN MEAM accumulates the pair potentials from only the first nearest neighbors, while 2NN MEAM includes the pair interactions from both the first and the second ones. In theory, for LI-MEAM, the pair potentials from arbitrary nearest neighbors can be included. However, in the practical implementation, a cutoff distance r_c is introduced to consider finite but enough nearest neighbors, as:

$$E^u(r) - F[\bar{\rho}^0(r)] = \frac{1}{2}\sum_{m=1}^{a_0^m r<r_c} Z_0^{(m)}\Phi(a_0^{(m)}r), \tag{11}$$

where $Z_0^{(m)}$ is the actual number of m-th nearest neighbors, $a_0^{(m)}$ is the ratio of the distance of m-th nearest neighbors to r, which is the distance for the first nearest neighbors. Besides, in order to improve the performance of the cutoff effect, a smooth radial cutoff function, $f_c[(r_c-r)/\Delta r]$ is used in LI-MEAM to handle on all the cutoff regions, where f_c is the smooth cutoff function given by:

$$f_c(x) = \begin{cases} 1, & x \geqslant 1 \\ [1-(1-x)^4]^2, & 0<x<1 \\ 0, & x \leqslant 0, \end{cases} \tag{12}$$

and Δr is the cutoff region. For present work, Δr was given 0.2 for all the elements.

In order to apply Chen–Möbius lattice inversion [17–21] on Eq. (11) to obtain the pair potential, the involved series $\{a_0^{(m)}\}$ should be firstly extended to a multiplicative semi-group $\{a^{(m)}\}$ such that, for any two integers i and j, an integer k always exists which satisfying:

$$a^{(i)}a^{(j)} = a^{(k)}. \tag{13}$$

Then Eq. (11) can be rewritten as:

$$E^u(r) - F[\bar{\rho}^0(r)] = \frac{1}{2}\sum_{m=1}^{a^{(m)}r<r_c} Z^{(m)}\Phi(a^{(m)}r), \tag{14}$$

Table 1
The leading 10 items of the related coefficient series of Chen–Möbius inverse formula for bcc structure.

m	1	2	3	4	5	6	7	8	9	10
$Z^{(m)}$	8	6	0	0	12	0	0	24	8	0
$a^{(m)}$	1.000	1.155	1.333	1.540	1.633	1.778	1.886	1.915	2.000	2.053
$I^{(m)}$	0.125	−0.094	0.070	−0.053	−0.188	0.040	0.281	−0.375	−0.125	−0.030

where

$$Z^{(m)} = \begin{cases} Z_0\left(a_0^{-1}\left[a^{(m)}\right]\right) & a^{(m)} \in \{a_0^{(m)}\} \\ 0 & a^{(m)} \notin \{a_0^{(m)}\} \end{cases}. \tag{15}$$

Note that $\{Z_0^{(m)}\}$ is the actual numbers of atoms in the m-th nearest neighbors, and $\{Z^{(m)}\}$ is the extended group which contains $\{Z_0^{(m)}\}$ with all the additive elements equal to zeros. If the left two items in Eq. (14) are regarded as one, it can be inverted to obtain the pair potential function by applying Chen–Möbius lattice inversion. The following equation shows the inverted function:

$$\Phi(r) = 2\sum_{m=1}^{a^{(m)}r<r_c} I^{(m)}\{E^u(a^{(m)}r) - F[\bar{\rho}^0(a^{(m)}r)]\}. \tag{16}$$

where the inversion coefficient $I^{(m)}$ is given by:

$$\sum_{a^{(m)}|a^{(k)}} I^{(m)} Z\left[a^{-1}\left(\frac{a^{(k)}}{a^{(m)}}\right)\right] = \delta_{k1}, \tag{17}$$

and δ_{k1} is Kronecker delta function. Noted that all the coefficients associated with lattice inversion are only structure dependent. Hence, for specific reference structure, one-time calculation is sufficient to determine all the related coefficients. Table 1 shows the leading 10 items of the related coefficient series of Chen–Möbius inverse formula for bcc structure, which can be used directly in the LI-MEAM.

Using Eq. (16), the pair potential can be obtained, which can be used in Eq. (1) to calculate the total energy of arbitrary systems.

3. Results and discussion

3.1. Determination of parameters

From the introduction above, a total of 12 parameters are involved for one single element in LI-MEAM potential, as the scaling factor A, the sublimation energy E_c, the equilibrium nearest-neighbor distance r_e, the bulk modulus B, the weighting factors $t^{(k)}$ (k = 1, 2, 3), the decay factors $\beta^{(k)}$ (k = 0, 1, 2, 3) and the cutoff distance r_c. Among the 12 parameters, E_c, r_e and B were given experimentally. As to $\beta^{(1)}$, $\beta^{(2)}$, $\beta^{(3)}$, some researchers have tried to optimize them so as to fit more physical properties [22,23]. However, to compare with those results of 1NN and 2NN MEAM [10,14], they were fixed at 1.0 for all the elements in present work. Therefore, only 6 parameters were needed to be determined for single element, *i.e.* A, $\beta^{(0)}$, $t^{(1)}$, $t^{(2)}$, $t^{(3)}$ and r_c.

In present work, all the bcc transition metals, as Fe, Cr, Mo, Nb, Ta, V, were investigated. To determine their individual potential parameters, some physical properties were chosen as the fitting targets so that their corresponding experimental values could be reproduced. Herein, elastic constants (C_{11}, C_{44}), vacancy formation energy (E_v^f), structure energy differences between bcc and fcc ($\Delta E_{bcc\to fcc}$), and between fcc and hcp ($\Delta E_{fcc\to hcp}$), surface energy of the lowest surface (1 1 0) ($E_{(110)}$), were selected. In consideration of the dependence of C_{12} on C_{11} and B for cubic systems, C_{12} was not taken into account as a fitting target. For the structure energy differences, all the available experimental data are thermodynamically assessed at room temperature using the calphad method [24]. Because it is difficult to obtain the surface energy of each surface in experiments and only the average surface energy for polycrystalline is available, we optimized the lowest surface energy ($E_{(110)}$) to approach the average value referring to previous works [13,14,25]. Besides, in order to make our results comparable to 2NN MEAM, the same experimental data in previous works [14] were adopted as the fitting targets to determine the parameters of LI-MEAM potential for individual elements.

Particle Swarm optimization (PSO) algorithm [22,23,26] was used to determine all the potential parameters simultaneously. The optimization procedure could be described as the following. The potential parameters, A, $\beta^{(0)}$, $t^{(1)}$, $t^{(2)}$, $t^{(3)}$ and r_c, were firstly given a set of initial values. Then the selected physical properties, C_{11}, C_{44}, $\Delta E_{bcc\to fcc}$, E_v^f, $E_{(110)}$, were calculated using this group of parameters based on LI-MEAM potential and the relative errors for each properties were calculated successively. A new group of parameters would be generated by PSO algorithm until the errors were acceptable. In order to guarantee the accuracy of some specified properties, different weighting factors were assigned to relevant errors. Besides, reasonable bounds were imposed on the parameters to ensure the physical correctness of the model. The effect of the potential parameters on individual properties for bcc transition metals was also investigated, as shown in Table 2. In the table, the plus sign means the effect is significant, the minus sign means the effect is minor, and no sign means no effect. From the table, A, $\beta^{(0)}$ and r_c have significant effect on almost every properties, while $t^{(1)}$, $t^{(2)}$, $t^{(3)}$ have no or slight effect on all the properties. So during the optimization, A, $\beta^{(0)}$ and r_c were more carefully determined than $t^{(1)}$, $t^{(2)}$, $t^{(3)}$.

Using the above optimization procedures, the parameters of individual elements for LI-MEAM potential could be determined, as listed in Table 3. In the table, the former six parameters,E_c, r_e, B, $\beta^{(1)}$, $\beta^{(2)}$, $\beta^{(3)}$, were fixed on experimental or specified values, and the latter six parameters, A, $\beta^{(0)}$, $t^{(1)}$, $t^{(2)}$, $t^{(3)}$, r_c, were optimized. By comparing the optimized cutoff distance with the distances of different nearest neighbors in the equilibrium structure for each element, it can be deduced that more than the second nearest neighbors are considered in our LI-MEAM potential. Specifically, the interactions of the third nearest neighbors were included for Cr, Mo and W, and up to the sixth nearest neighbors were included for Fe, V, Nb and Ta. Fig. 1 shows the inverted pair potential changing with the nearest neighbor distance for all the bcc transition metals.

Table 2
Effect of parameters on individual properties for bcc transition metals. The plus sign means the effect is significant, the minus sign means the effect is minor, and no sign means no effect.

	A	$\beta^{(0)}$	$t^{(1)}$	$t^{(2)}$	$t^{(3)}$	r_c
C_{11}	+	+	No	–	No	+
C_{44}	+	+	No	–	No	+
E_v^f	+	+	–	–	–	+
$E_{(110)}$	+	–	–	–	No	–
$\Delta E_{bcc\to fcc}$	+	+	No	No	No	+
$\Delta E_{fcc\to hcp}$	+	+	No	No	No	+

Table 3
Optimized parameters of Fe, Cr, Mo, Nb, Ta, V and W using LI-MEAM potential. Values listed are the sublimation energy E_c (eV), the equilibrium nearest-neighbor distance r_e (Å), the bulk modulus $B(10^{12}$ dyn/cm$^2)$, the exponential decay factors for the atomic densities $\beta^{(0)}$, $\beta^{(1)}$, $\beta^{(2)}$, $\beta^{(3)}$, the scaling factor for the embedding energy A, the weighting factors for the atomic densities $t^{(1)}$, $t^{(2)}$, $t^{(3)}$, and the cutoff distance r_c. The former six parameters were fixed on experimental or specified values and the latter six ones were optimized.

	E_c	r_e	B	$\beta^{(1)}$	$\beta^{(2)}$	$\beta^{(3)}$	A	$\beta^{(0)}$	$t^{(1)}$	$t^{(2)}$	$t^{(3)}$	r_c
Fe	4.29	2.480	1.732	1.000	1.000	1.000	0.411	3.515	−5.023	7.233	−6.972	5.905
Cr	4.10	2.495	1.900	1.000	1.000	1.000	0.341	3.067	−2.527	12.072	−4.894	4.471
Mo	6.81	2.725	2.650	1.000	1.000	1.000	0.356	3.551	−1.158	−5.183	1.186	4.881
W	8.66	2.740	3.140	1.000	1.000	1.000	0.305	2.973	−4.065	−3.110	−6.895	4.908
V	5.30	2.625	1.570	1.000	1.000	1.000	0.442	3.349	0.538	−5.517	−3.352	6.249
Nb	7.47	2.860	1.730	1.000	1.000	1.000	0.466	3.391	0.291	−8.696	2.828	6.805
Ta	8.09	2.860	1.940	1.000	1.000	1.000	0.370	3.204	−3.093	−6.266	−8.050	6.807

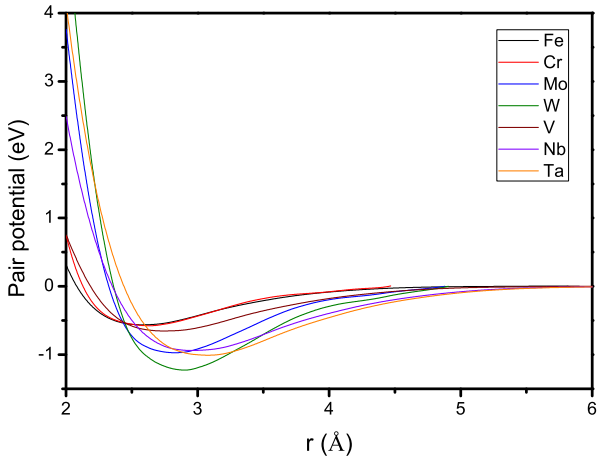

Fig. 1. Inverted pair potential changing with the nearest neighbor distance for all the bcc transition metals.

Table 4
Calculated elastic constants $(10^{12}$ dyn/cm$^2)$ using LI-MEAM potential, in comparison with experimental data and those calculated by 2NN MEAM. All the experimental data are from Ref. [27].

	C_{11}			C_{12}			C_{44}		
	Expt.	2NN	LI	Expt.	2NN	LI	Expt.	2NN	LI
Fe	2.431	2.430	2.431	1.381	1.380	1.377	1.219	1.219	1.219
Cr	3.910	3.909	3.909	0.896	0.897	0.901	1.032	1.034	0.879
Mo	4.647	4.649	4.647	1.615	1.655	1.659	1.089	1.088	1.089
W	5.326	5.326	5.326	2.050	2.050	2.047	1.631	1.631	1.632
V	2.324	2.323	2.324	1.194	1.194	1.191	0.460	0.460	0.460
Nb	2.527	2.527	2.527	1.332	1.331	1.333	0.310	0.319	0.310
Ta	2.663	2.664	2.663	1.582	1.581	1.585	0.874	0.875	0.874

3.2. Calculation of physical properties

To evaluate the reliability of the developed LI-MEAM potential and the optimized potential parameters, various physical properties of individual elements were calculated using the optimized parameters. Except the properties used for fitting, some other energetic properties were also calculated, such as formation energies of surfaces (100) and (111), $E_{(100)}$ and $E_{(111)}$, structure energy differences between bcc and sc, $\Delta E_{bcc\to sc}$, and between bcc and diamond, $\Delta E_{bcc\to dia}$, the activation energy of vacancy diffusion, Q, and some thermal properties which include thermal expansion coefficient, ε, specific heat, C_p, bulk melting point, T_{bm}, latent heat of melting, ΔH_m, and volume change on melting, $\Delta V_m/V_{solid}$. In this subsection, the calculated values of these properties were listed together with the corresponding experimental data and those calculated by 2NN MEAM as comparisons.

Table 4 shows the calculated and the experimental elastic constants (C_{11}, C_{12} and C_{44}) for individual elements. Elastic constants were given higher weights during the optimization procedures so that these basic materials properties could be accurately reproduced. From the table, almost all the elastic constants for all the bcc transition metals agree excellently with the corresponding experimental data. The only exception among these calculated results is C_{44} of Cr, this is because that we sacrifice a slight accuracy of C_{44} to guarantee higher accuracy of both the surface energies and the vacancy formation energy.

The calculated and available experimental structural energy differences among various crystal structures are listed in Table 5. Among these items, $\Delta E_{bcc\to fcc}$ and $\Delta E_{fcc\to hcp}$ were used for fitting, and the other two were predicted. As mentioned above, all the available experimental data were thermodynamically assessed at room temperature using the calphad method [24]. From the table, it can be seen that the structural energy of bcc crystal for all the elements is lower than that of any other crystals, which demonstrates the correct prediction of the ground state. Quantitatively speaking, for most of the concerned elements, the values of $\Delta E_{bcc\to fcc}$ and $\Delta E_{fcc\to hcp}$ calculated by LI-MEAM potential are very close to the corresponding experimental data, while for Cr, the accuracy of $\Delta E_{fcc\to hcp}$ was sacrificed to better fit both the vacancy formation energy and surface energies. As for $\Delta E_{bcc\to sc}$ and $\Delta E_{bcc\to dia}$, no experimental results were available. The calculated results based on LI-MEAM potential are compared with those from 2NN MEAM. It can be seen that without the many-body screening function and two less parameters, LI-MEAM achieved similar accuracy levels as 2NN MEAM, which validates the correctness of optimized parameters.

Then the vacancy formation energy, E_v^f, and the activation energy of vacancy diffusion, Q, of individual elements are presented in Table 6, together with the corresponding experimental data and those from 2NN MEAM. In the table, the vacancy formation energy was used as one of the fitting targets and the activation energy of vacancy diffusion, which is the sum of the vacancy formation energy and the vacancy migration energy, was predicted. As can be seen from the table, the vacancy formation energies calculated by LI-MEAM are in excellent agreement with experimental data for all the elements, which is better than those of 2NN MEAM. As for the activation energy of vacancy diffusion, most of the calculated values by LI-MEAM are closer to the experimental data than those of 2NN MEAM, except that those of Cr and W are slightly larger. Therefore, in terms of vacancy defects, LI-MEAM exhibits comparable performance than 2NN MEAM.

Table 7 lists the calculated surface energies of the three low-index surfaces (100), (110), and (111), as $E_{(110)}$, $E_{(100)}$, $E_{(111)}$ using LI-MEAM, in comparison with experimental data and those of 2NN MEAM. In the table, the experimental values are surface energies for individual polycrystalline solids, which are extrapolated values, directly from high-temperature experimental data to 0 K [31,32]. As mentioned above, only the lowest surface energy [that of (110) surface] was fitting to the experimental surface energy and no constraints were applied on the order of the surface energies. From the table, LI-MEAM could predict correct order among the

Table 5
Calculated structural energy differences ΔE (eV), using LI-MEAM potential, in comparison with experimental data and those calculated by 2NN MEAM. All the experimental data are thermodynamically assessed values at room temperature [24].

	$\Delta E_{bcc\to fcc}$			$\Delta E_{fcc\to hcp}$			$\Delta E_{bcc\to sc}$		$\Delta E_{bcc\to dia}$	
	Expt.	2NN	LI	Expt.	2NN	LI	2NN	LI	2NN	LI
Fe	0.082	0.069	0.051	−0.023	−0.023	−0.022	0.99	0.71	1.82	1.76
Cr	0.075	0.070	0.092	−0.029	−0.029	−0.008	1.32	0.70	1.50	2.01
Mo	0.158	0.167	0.158	−0.038	−0.038	−0.040	1.97	1.31	2.37	3.39
W	0.200	0.263	0.188	−0.047	−0.047	−0.040	2.61	1.64	3.70	4.41
V	0.078	0.084	0.068	−0.036	−0.011	−0.034	0.78	0.70	1.22	1.96
Nb	0.140	0.176	0.105	−0.036	−0.012	−0.054	0.90	0.95	1.44	2.84
Ta	0.166	0.148	0.115	−0.041	−0.023	−0.062	1.32	1.24	2.51	3.31

Table 6
Calculated vacancy formation energy E_v^f (eV) and activation energy of vacancy diffusion Q (eV), using LI-MEAM potential, in comparison with experimental data and those calculated by 2NN MEAM. The experimental vacancy formation energies are from Ref. [28] and the experimental activation energies of diffusion are from Ref. [29], except for the activation energy of diffusion for Cr, which is from Ref. [30].

	E_v^f			Q		
	Expt.	2NN	LI	Expt.	2NN	LI
Fe	1.79	1.75	1.79	2.5	2.28	2.39
Cr	1.80	1.91	1.80	3.1	2.61	2.51
Mo	3.10	3.09	3.10	4.5	4.22	4.41
W	3.95	3.95	3.95	5.5	5.56	5.71
V	2.10	2.09	2.10	3.2	2.47	2.74
Nb	2.75	2.75	2.75	3.6	3.32	3.83
Ta	2.95	2.95	2.95	4.3	3.71	4.60

Table 7
Calculated surface energies (erg/cm^2) of three low-index surfaces (1 0 0), (1 1 0), and (1 1 1), as $E_{(110)}$, $E_{(100)}$, $E_{(111)}$, using LI-MEAM potential, in comparison with experimental data and those calculated by 2NN MEAM. The experimental values, E_{poly}^{expt}, are for corresponding polycrystalline solids and are extrapolated from high-temperature experimental data to 0 K (Fe and W are from Refs.[31] and the others are from Ref. [32]).

	Expt.	$E_{(110)}$		$E_{(100)}$		$E_{(111)}$	
		2NN	LI	2NN	LI	2NN	LI
Fe	2360	2356	2358	2510	2749	2668	2799
Cr	2200	2198	2200	2300	2394	2501	2868
Mo	2900	2885	2825	3130	3138	3373	3584
W	2990	3427	3646	3900	4158	4341	4846
V	2600	2636	2600	2778	2745	2931	3149
Nb	2300	2490	2382	2715	2682	2923	3188
Ta	2780	2778	2909	3035	3387	3247	3845

three low-index surface energies, as $E_{(110)} < E_{(100)} < E_{(111)}$. Meanwhile, the calculated $E_{(110)}$ of individual elements agree well with corresponding experimental data except that of W, which is somewhat larger.

Finally, Table 8 shows the calculated and experimental thermal properties, which include thermal expansion coefficient ε, specific heat C_p, bulk melting point T_{bm}, latent heat of melting ΔH_m and volume change on melting $\Delta V_m/V_{solid}$. Here, the thermal expansion coefficient and the specific heat were calculated with the temperature ranging from 0 °C to 100 °C, the melting points were calculated using the solid–liquid interface-based method, [33] while the latent heat of melting and the volume change of melting were calculated based on the direct heating process. From the table, it can be seen that almost all the calculated values of thermal expansion coefficient, specific heat and the latent heat of melting for individual elements (except the thermal expansion coefficient of Mo and the latent heat of melting of Fe) are smaller than the corresponding experimental data, while for those of bulk melting point, they are somewhat larger than the experimental values. The consistency of the trends of these results reflects the stability and robustness of LI-MEAM potential model and the optimized parameters. Besides, compared with the results calculated by 2NN MEAM, most of those values by LI-MEAM are closer to the experimental data, especially for the bulk melting point and the latent heat of melting. As to the volume change of melting, no experimental values are available except for Fe. However, the values calculated by 2NN MEAM and LI-MEAM are with similar levels except for those of V, Nb and Ta. Lee believed that the volume change values of V and Nb calculated by 2NN MEAM were relatively small [14], so it is believed that those presented by LI-MEAM should be more reasonable.

To clearly illustrate the deviation of the calculated values of various physical properties by LI-MEAM potential from the corresponding experimental values, and easily compare with those by 2NN MEAM, Fig. 2 was drawn. In the figure, the horizontal axis represents the various physical properties discretely, which are labeled by circled numbers, and the vertical axis represents the ratios of the calculated values of various physical properties to the corresponding experimental values. Thus, the closer the calculated curve is to the dashed line in the figure, the better the optimized parameters are. Besides, the black curves in the figure are for 2NN MEAM and red ones are for LI-MEAM. Based on this understanding, it can be found that the physical properties of Mo were predicted with good accuracy. Concerning W and V, the perfor-

Table 8
Calculated thermal properties, using LI-MEAM potential, in comparison with experimental data and those of 2NN MEAM. Values listed are the thermal expansion coefficient ε (10^{-6}/K), specific heat C_p (J/mol K), melting point of individual bulk material T_{bm} (K), latent heat of melting ΔH_m (kJ/mol) and volume change of melting $\Delta V_m/V_{solid}$ (%). The experimental data for thermal expansion coefficient, specific heat and volume change are from Ref. [29] and others are from Ref. [24].

	ε (0–100 °C)			C_p (0–100 °C)			T_{bm}			ΔH_m			$\Delta V_m/V_{solid}$		
	Expt.	2NN	LI	Expt.	2NN	LI	Expt.	2NN	LI	Expt.	2NN	LI	Expt.	2NN	LI
Fe	12.1	12.4	9.5	25.5	26.1	24.3	1811	2200	2059	13.8	13.2	14.1	3.5	3.4	4.2
Cr	6.5	9.0	6.2	24.0	26.8	23.1	2180	2050	2427	21.0	18.8	19.2	–	4.4	4.9
Mo	5.1	5.3	5.3	24.1	25.9	23.8	2896	3100	3210	37.5	20.1	31.0	–	3.0	5.0
W	4.5	4.2	3.8	25.4	25.4	24.4	3695	4600	4045	52.3	33.0	35.3	–	3.2	4.5
V	8.3	8.7	6.2	25.4	26.1	24.6	2183	1800	2276	21.5	11.7	15.9	–	1.3	3.3
Nb	7.2	6.4	4.8	24.9	26.1	24.8	2750	1900	3030	30.0	13.5	21.9	–	1.0	3.3
Ta	6.5	5.8	5.8	25.7	25.7	24.2	3290	3200	3615	36.6	22.3	29.0	–	2.1	4.4

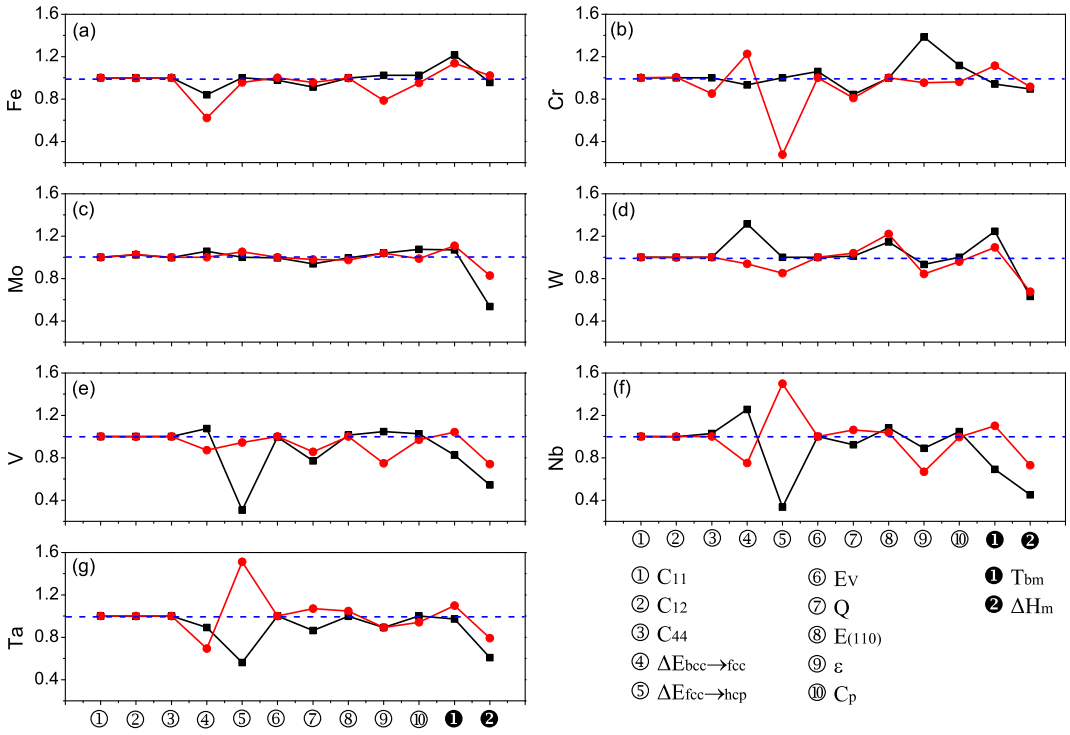

Fig. 2. Scaled values of the various physical properties by 2NN MEAM (lines in black and LI-MEAM (lines in red) by the corresponding experimental values for individual elements. For aesthetic reasons, the labels of the horizontal axis, which represent the names of physical properties, are replaced by circled numbers and demonstrated aside. (For interpretation of the references to color in this figure legend, the reader is referred to the web version of this article.)

mance of present LI-MEAM is also pretty good except for some small deviations, which is better than that of 2NN MEAM. As for Fe, Cr, Nb, Ta, some relatively big deviations exist on the structural energy differences for both 2NN MEAN and LI-MEAM. Overall, compared with 2NN MEAM, LI-MEAM for bcc transition metals shows competitive performance.

To summary, based on the calculated results shown in Tables 4–8 and Fig. 2, the LI-MEAM potential, a simplified version of previous model, were validated as a universal and accurate potential model again. Meanwhile, the optimized potential parameters for LI-MEAM could be used to calculate various physical properties which agree well with experimental data. This also reveals the possibility of applying the optimized parameters based on LI-MEAM potential to more comprehensive systems and achieving relatively high accuracy.

4. Conclusions

In present work, we applied the LI-MEAM potential to all the bcc transition metals, as Fe, Cr, Mo, W, V, Nb, and Ta. By fitting to some selected physical properties, as elastic constants, structural energy differences among bcc, fcc and hcp structures, vacancy formation energy and surface energy of (110) surface, the potential parameters of individual elements, were parameterized using particle swarm optimization method. Besides, more physical properties of individual elements, including structural energy differences among bcc, sc and diamond structures, the activation energy of vacancy diffusion, surface energies of (100) and (111) surfaces and some thermal properties (thermal expansion coefficient, specific heat, bulk melting point, latent heat of melting and volume change on melting), were calculated and compared with experimental data and those calculated by 2NN MEAM. It is shown that the present potentials could reasonably predict most of the properties of the bcc transition metals. The good agreement proves the reliability of the proposed LI-MEAM potential formalism, as well as the optimized parameters. Based on the present results, it is believed the optimized parameters of LI-MEAM potential could be implemented into wide applications.

Acknowledgements

The authors gratefully thank Prof. Nanxian Chen, Prof. Jiang Shen for helpful discussions about Chen–Möbius lattice inversion. This work is supported by the National Basic Research Program of China (2011CB606401 and 2013CB934800), National Natural Science Foundation of China (51101064 and 51302094) and Research Funds by State Key Laboratory of Material Processing and Die & Mould Technology, Huazhong University of Science and Technology. We thank the technology support by the Texas Advanced Computing Center (TACC) at the University of Texas at Austin (http://www.tacc.utexas.edu) for providing grid resources that have contributed to the research results reported within this paper.

References

[1] F.F. Abraham, R. Walkup, H. Gao, M. Duchaineau, T.D.D.L. Rubia, M. Seager, Proc. Nat. Acad. Sci. USA 99 (2002) 5777.
[2] D.E. Shaw, P. Maragakis, K. Lindorff-Larsen, S. Piana, R.O. Dror, M.P. Eastwood, J.A. Bank, J.M. Jumper, J.K. Salmon, Y. Shan, W. Wriggers, Science 330 (2010) 341.
[3] J.H. Li, X.D. Dai, S.H. Liang, K.P. Tai, Y. Kong, B.X. Liu, Phys. Rep. 455 (2008) 1.
[4] M.S. Daw, M.I. Baskes, Phys. Rev. Lett. 50 (1983) 1285.
[5] M.W. Finnis, J.E. Sinclair, Philos. Mag. A 50 (1984) 45.
[6] F.H. Stillinger, T.A. Weber, Phys. Rev. B 31 (1985) 5262.
[7] J. Tersoff, Phys. Rev. B 37 (1988) 6991.
[8] R.A. Johnson, Phys. Rev. B 37 (1988) 3924.
[9] M.I. Baskes, J.S. Nelson, A.F. Wright, Phys. Rev. B 40 (1989) 6085.
[10] M.I. Baskes, Phys. Rev. B. 46 (1992) 2727.
[11] M. Doyama, Y. Kogure, Comput. Mater. Sci. 14 (1999) 80.
[12] M.I. Baskes, Mater. Chem. Phys. 50 (1997) 152.
[13] B.-J. Lee, M.I. Baskes, Phys. Rev. B 62 (2000) 8564.

[14] B.-J. Lee, M.I. Baskes, H. Kim, Y.K. Cho, Phys. Rev. B 64 (2001) 184102.
[15] B.-J. Lee, J.-H. Shim, M.I. Baskes, Phys. Rev. B 68 (2003) 144112.
[16] J.H. Rose, J.R. Smith, F. Guinea, J. Ferrante, Phys. Rev. B 29 (1984) 2963.
[17] N.X. Chen, Phys. Rev. Lett. 64 (1990) 1193.
[18] Q. Xie, M.C. Huang, J. Phys. Condens. Matter. 6 (1994) 11015.
[19] N.X. Chen, Z.D. Chen, Y.C. Wei, Phys. Rev. E 55 (1997) 5.
[20] S. Zhang, N. Chen, Phys. Rev. B 66 (2002) 064106.
[21] Z.W. Cui, Y. Sun, Y.J. Chen, J.M. Qu, Solid State Ionics 187 (2011) 8.
[22] Z.W. Cui, F. Gao, Z.H. Cui, J.M. Qu, Modell. Simul. Mater. Sci. Eng. 20 (2012) 15014.
[23] Z.W. Cui, F. Gao, Z.H. Cui, J.M. Qu, J. Power Sources 207 (2012) 150.
[24] A.T. Dinsdale, CALPHAD: Comput. Coupl. Phase Diagrams Thermochem. 15 (1991) 317.
[25] X.-Y. Yuan, N.-X. Chen, J. Shen, W. Hu, J. Phys. Condens. Matter. 22 (2010) 375503.
[26] J. Kennedy, R. Eberhart, IEEE Trans. Neural Networks (1995) 1942.
[27] P. Bujard, Ph.D. thesis, University of Geneva, 1982.
[28] B. Zhang, Y. Ouyang, S. Liao, Z. Jin, Physica B 262 (1999) 218. and references therein.
[29] E.A. Brandes, G.B. Brook (Eds.), Smithells Metals Reference Book, seventh ed., Butterworth-Heinemann, Oxford, 1992.
[30] J. Askill, G.H. Tomlin, Philos. Mag. 11 (1965) 467.
[31] W.R. Tyson, W.A. Miller, Surf. Sci. 62 (1977) 267.
[32] M.I. Baskes, B. Hyland, Private Communication.
[33] J. Morris, C. Wang, K. Ho, C. Chan, Phys. Rev. B 49 (1994) 3109.